Arabian Journal for Science and Engineering
https://doi.org/10.1007/s13369-023-07647-6

RESEARCH ARTICLE-CIVIL ENGINEERING

Evaluation of the Performance Limit States in Codes for RC Columns Under Different Axial Loads

Ilker Subasi[1,3] · Naci Caglar[2,4] · M. Nadir Olabi[2] · Huseyin Kasap[2]

Received: 28 January 2022 / Accepted: 18 January 2023

Abstract
Reinforced concrete columns that are not designed according to current seismic codes may be damaged under the earthquakes loads, which may cause the reinforced concrete buildings to collapse. The response of RC columns subjected to earthquake loads has to be examined in order to determine the seismic performance of RC buildings. The performance of RC columns is determined by using the deformation-based performance limit values given in the seismic codes. In this study, the effectiveness of performance limits proposed for RC columns in current seismic codes is examined quantitatively. A nonlinear finite element model was developed and verified using results of experimental studies selected from the literature. A parametric study was carried out to evaluate the performance of the state limits proposed in the codes. It is concluded that the performance limits values in TBEC 2018 are generally quite conservative compared to the values in Eurocode 8 and ASCE 41–17. This was clearly seen in low axial load levels where the effective performance is restricted to 22–53% of the actual column capacity, which limits the use of the potential ductile behavior in columns dominant by flexural response. Moreover, the study shows that the axial load level is a very important parameter in determining the performance levels according to the standards, and it is recommended that the codes used in the study update their performance levels to consider axial load variation effects.

Keywords Performance limits · Seismic performance · RC columns · Nonlinear finite element model · Axial load ratio · Ductility

List of Symbols

A_g	Gross cross-sectional area
A_{shx}	Area of the horizontal reinforcement parallel to the loading direction
A_{sl}	Tension longitudinal bars area
A_v	Transverse reinforcement area
α	Confinement effect factor
α_{ASCE}	Coefficient in ASCE-SEI 41–17
α_{col}	Coefficient depending on the s/d_{eff} ratio
a_v	Coefficient is taken as 1 if the shear fracture exceeds flexural fracture; otherwise, it is taken as 0
b	Width of column
b_{ASCE}	Coefficient in ASCE-SEI 41–17
b_c	Width of the core concrete measured from the centers of the stirrups
b_i	Distance between the centers of the horizontal reinforcement and the adjacent supported longitudinal reinforcement
d	Depth of column
d'	Compressive reinforcement depth
d_{bl}	Diameter of the tension reinforcement
d_c	Depth of the core concrete measured from the centers of the stirrups
d_{eff}	Effective section depth
d_h	Horizontal bar diameter
d_l	Longitudinal bar diameter
E_s	Modulus of elasticity steel bars
EI_{flex}	Flexural stiffness
f_{cc}	Confined concrete peak stress

✉ Naci Caglar
caglar@sakarya.edu.tr

1 Department of Civil Engineering, Faculty of Engineering and Architecture, Istanbul Arel University, 34537 Istanbul, Türkiye

2 Department of Civil Engineering, Faculty of Engineering, Sakarya University, 54050 Sakarya, Türkiye

3 Department of Civil Engineering, Institute of Natural Sciences, Sakarya University, 54050 Sakarya, Türkiye

4 Department of Civil Engineering, Faculty of Engineering and Natural Sciences, Bursa Technical University, 16310 Bursa, Türkiye

Published online: 11 February 2023

f_{co}	Unconfined concrete compressive strength
f_{su}	Steel bars ultimate stress
f_{sy}	Steel bars yield stress
f_{uh}	Ultimate strength of horizontal reinforcement
f_{ul}	Ultimate strength of longitudinal reinforcement
f_{yh}	Yield strength of horizontal reinforcement
f_{yl}	Yield strength of longitudinal reinforcement
k	Coefficient depending on the displacement ductility
k_{slip}	Slip stiffness
L	Length of column
L_p	Length of plastic hinge
L_s	Shear span (moment/shear force ratio)
M	Moment
M_y	Yield moment strength
P	Axial load
s	Horizontal reinforcement step distance
u	Average bond stress
V	Shear force
V_{cr}	Lateral load at shear cracking
V_{max}	Maximum lateral load
V_n	Maximum shear strength
V_o	Shear capacity
V_p	Maximum flexure strength
V_y	Shear demand at flexural yielding
w	Mechanical reinforcement ratio of tension reinforcement
$w^{'}$	Mechanical reinforcement ratio compressive reinforcement
z	Length of section internal lever arm
γ_{el}	Coefficient taken as 1.5 for a primary seismic element and 1 for a secondary seismic element
Δ	Total displacement at column
Δ_{ALF}	Maximum flexure and shear displacement from the total lateral displacement at shear model proposed by Sezen
Δ_{af}	Displacement at axial load failure at shear model proposed by Sezen
Δ_{cr}	Displacement at shear cracking at shear model proposed by Sezen
$\Delta_{flexure}$	Flexure deformation
Δ_{max}	Displacement corresponding maximum lateral load
Δ_n	Displacement value at the maximum strength at shear model proposed by Sezen
Δ_u	Displacements at ultimate load (80% of V_{max})
Δ_{us}	Deformation value at the moment when the shear strength starts to decrease at shear model proposed by Sezen
Δ_{shear}	Shear deformation
Δ_{slip}	Slip deformation
Δ_y	Displacements at yield
ε	Strain
ε_{cc}	Confined concrete with a peak stress corresponding strain
ε_{co}	Unconfined concrete with a peak stress corresponding strain (0.002)
ε_{cu}	Confined concrete ultimate strain
ε_{su}	Steel bars ultimate strain
ε_{sy}	Steel bars yield strain
ϕ_u	Ultimate curvature
ϕ_y	Yield curvature
θ	Chord rotation
θ_a	Angle of the shear fracture (0.65)
θ_p^{CD}	Plastic rotation limit for controlled damage performance level
θ_p^{CP}	Plastic rotation value allowed for performance level of collapse prevention
θ_y	Rotation at yield
λ	Coefficient for slightly aggregated concrete or regular aggregated concrete
ϑ	Axial load ratio (ALR)
ρ_d	Diagonal reinforcement ratio
ρ_h	Ratio of horizontal reinforcement area to gross concrete area perpendicular to that reinforcement
ρ_{hx}	Ratio of stirrups parallel to the loading direction
ρ_l	Longitudinal reinforcement ratio
σ	Stress
η	Coefficient by element type

1 Introduction

Vertical load-bearing elements of reinforced concrete (RC) buildings in regions with seismic ground motion react under the influence of both axial load and large lateral forces during earthquakes. RC elements that are not designed in accordance with current codes could be damaged by the axial and lateral loads acting on them during an earthquake, which can cause the RC structures to collapse [1]. In order to be able to determine the seismic performance of RC buildings during earthquakes, the behavior of RC columns subjected to earthquake loads has to be examined. Therefore, the deformation-based performance limit values available in the seismic codes are used to determine the performance of RC columns.

Generally, two ways are used by researchers to determine the behavior of reinforced columns (RC). The first is performing an experimental in-the-lab tests, and the other is to implement analytical and numerical modeling verified against experiment work. For example, Acun and Sucuoglu [2] experimentally tested conforming and nonconforming columns under lateral and constant axial loads. The performance levels of the columns subjected to the test were determined according to Eurocode 8, ASCE-SEI 41–06, and TEC 2007 [3–5]. All three codes gave similar results for the minimum damage and yield limit states, but on the other

hand, different results for life safety and collapse prevention performance limits were noticed. Similarly, Elci and Goker [6] examined, experimentally and numerically, the earthquake performance of RC columns according to TEC 2007 and TBEC 2018 [7] codes. It was stated that the experimental results and the findings obtained from sectional analysis were compatible with each other. Moreover, the performance limit values were compared according to the TEC 2007 and TBEC 2018 codes, and the researchers concluded that the TBEC 2018 code gives performance limit values that are on the safe side. Nevertheless, due to the recent updates on ASCE-SEI 41 and Turkish code, it would be useful to analytically reexamine the aforementioned studies outcomes based on the new version of the codes and with various axial load levels and different characteristics of RC columns. Extendedly, by utilizing a database of 65 rectangular and circular columns, Opabola and Elwood [8] investigated the collapse mode and deformation capacity according to ASCE-SEI 41–13 [9] and ASCE-SEI 41–17 [10]. The researchers found out that the general curvature-based method in the New Zealand code could not accurately determine the collapse mode and gives a more conservative estimate compared to ASCE-SEI 41–17. A direct rotation-based approach and a rocking model were proposed [11] to reduce the conservatism of the current method. However, the outcomes presented in this work were made according to columns that did not demonstrate a ductile behavior.

Researchers also studied the capacities of full-scale RC frames, both experimentally and analytically [12, 13]. Although the experimental results conducted by Tore et al. [12] were compared to the shear capacity models from ASCE/SEI 41–17, Eurocode 8, and TBEC 2018, limit state investigation was not carried on. On the other hand, Jamal and Yuksel [13] performed a numerical pushover analysis using plastic hinge characteristics according to TBEC 2018 and ASCE-SEI 41–17 standards. It was concluded that the peak displacement, base shear force and floor shear force values calculated according to TBEC 2018 are higher than the values calculated according to ASCSEI 41–17. However, the conclusions were based on analytical results only without comparing or verifying with experimental studies.

Analytical studies found in the literature, to the knowledge of the authors, did not consider the comparison of the performance limit values in the modern and widely used codes Eurocode 8, TBEC 2018, and ASCE 41–17 altogether. Foroughi and Yuksel [14] performed a parametric numerical study on square, rectangular and circular RC columns analyzed using the strain-based damage limits according to TBEC 2018. In other work (Foroughi and Yuksel [15]), researchers evaluated only circular columns to check the adequacy of the deformation and damage limit levels given in both ASCE-SEI 41–17 and TBEC 2018 codes. In these studies, the nonlinear response of the columns was determined using concentrated plasticity based on moment–curvature analysis where shear and slip behavior was ignored. For that matter, it will be more convenient to examine the performance targets of columns designed following current codes under cycle loading, while taking flexural, shear and slip behaviors into account.

The main objective of this study is to examine the effectiveness of the deformation-based performance limit states proposed by Eurocode 8, ASCE-SEI 41–17, and TBEC 2018 in determining the performance of RC columns under earthquake loading and subjected to variant axial load levels. In addition, determining the effects of cross-sectional dimensions and axial load ratios on performance levels of reinforced concrete columns demonstrated in the codes are important goals of this work. To achieve this purpose, a nonlinear finite element model is created based on OpenSees [16] framework, and verified with the results of experimental studies selected from the literature [17, 18]. Furthermore, using the validated numerical model, the behavior of RC columns under constant axial load and cyclic loading is examined by utilizing a parametric study. Also, the results were compared with the deformation-based performance limit values recommended by the relevant codes.

2 Referenced Experimental Studies

Two specimens from Sezen [17] and three specimens from Lynn et al. [18] are used in the scope of this study to validate the nonlinear finite element model of RC columns. Sezen analyzed the causes of the collapse of real-scale columns under the effect of axial load and lateral loading. The experimental setup prepared by Sezen was constructed with nearly rigid top and base beams to provide a double curvature deformations. Lynn et al. emphasized that the RC columns built before 1970 were damaged due to flexural, shear, and lack of connection in the reinforcements, and the behavior of such columns under the effect of axial and lateral loading was examined. Both of these studies used the same experimental setup which is illustrated in Fig. 1. In this setup, the axial load was applied to the column specimens by two hydraulic actuators, A and B, and lateral displacement was applied by the actuator C. Also, out of plane displacements that may occur during the test were prevented by an additional support frame. Table 1 presents the properties of the five test specimens selected for this work in terms of the width of column b, depth d, length L, concrete compressive strength f_{co}, longitudinal reinforcement yield strength f_{yl}, longitudinal bar diameter d_l, yield strength of horizontal reinforcement f_{yh}, horizontal bar diameter d_h, horizontal reinforcement step distance s, and P the axial load value. The cross-sectional information of the test samples is given in Fig. 2.

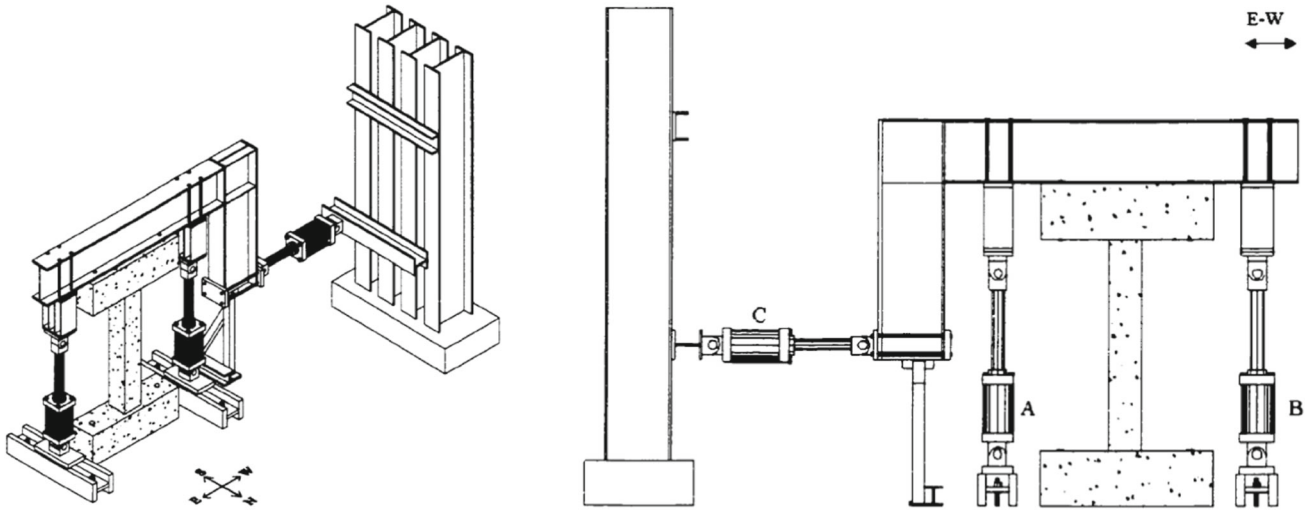

Fig. 1 Experimental test setup [17]

Table 1 Referenced column properties

	Column name	L(mm)	f_{co}(MPa)	f_{yl}* (MPa)	f_{ul}* (MPa)	d_l(mm)	f_{yh}* (MPa)	f_{uh}* (MPa)	d_h(mm)	s(mm)	ALR
Sezen [16]	Specimen-1	2946.4	21.1	434.3	644.0	28.5	475.6	723.0	9.5	304.8	0.15
	Specimen-2	2946.4	21.1	434.3	644.0	28.5	475.6	723.0	9.5	304.8	0.60
Lynn et al. [17]	2CLH18	2946.4	33.1	330.8	482.0	25.4	400.0	534.0	9.5	457.2	0.07
	3CLH18	2946.4	25.6	330.8	482.0	32.3	400.0	534.0	9.5	457.2	0.09
	3CMD12	2946.4	27.6	330.8	482.0	32.3	400.0	534.0	9.5	304.8	0.26

* Grade 40 deformed bars, $ALR(\vartheta) = P/\left(f_{co}A_g\right)$

Fig. 2 Cross sections of reference experiments (mm)

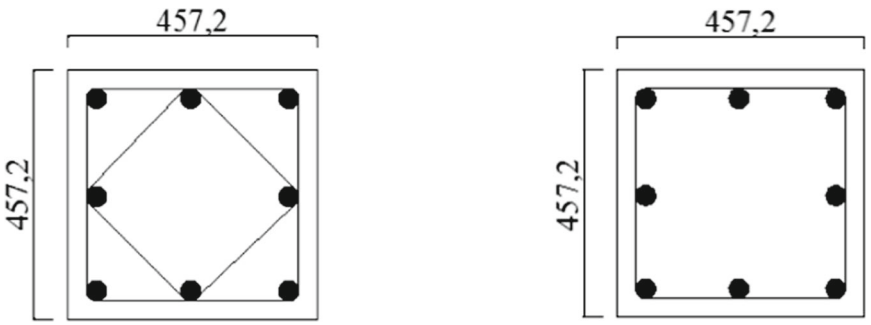

a) Specimen-1, Specimen-2 and 3CMD12 b) 3CLH18 and 2CLH18

3 Modeling the Nonlinear Behavior of RC Columns

Macro-level modeling techniques are capable of simulating the actual behavior of RC elements like shear walls and RC columns [19–22]. These kinds of approaches are very low on resources and simpler to prepare and utilize compared to the detailed finite element models (FEM). However, capturing the real response of RC elements requires special care while selecting the constitutive models that represent the expected nonlinear multi-phenomena controlling the behavior of the studied member.

3.1 Flexural Response

In this study, the Fiber Beam-Column Element Model (FBCEM) developed by Spacone et al. [23] is adapted to simulate the flexural behavior of the reference RC columns and later on to perform the parametric study. In this model, five integration points are selected in a force-based formulation

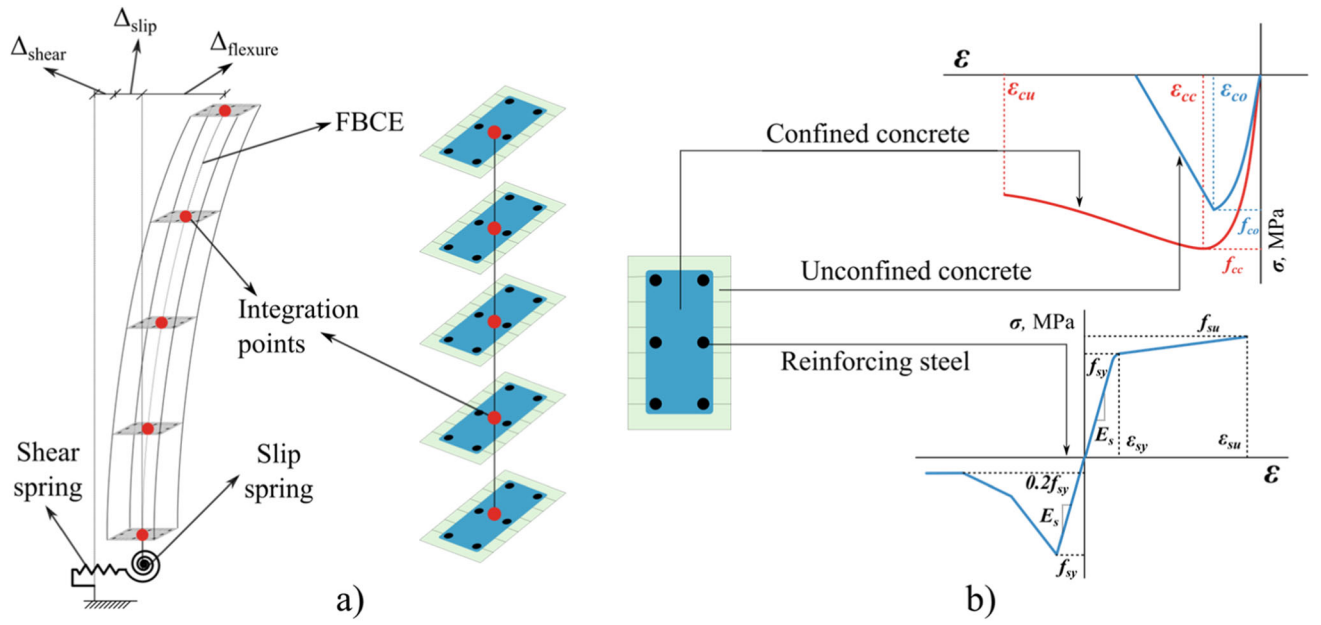

Fig. 3 **a** Fiber Beam-Column Element Model **b** Material Models

found in the OpenSees library [24], where forces and displacements are calculated by performing integrals at section level at each integration point (Fig. 3a). The column section is divided into three kinds of fibers representing the confined, unconfined concrete and reinforcement steel bars.

Kent and Park [25]-based uniaxial material Concrete01, from the OpenSees library, is assigned to the unconfined concrete with a peak stress equal to the compressive strength of the concrete, f_{co}, and a corresponding strain $\varepsilon_{co} = 0.002$. Concrete04 uniaxial material is assigned to the confined concrete, where peak stress (f_{cc}) and strain (ε_{cc}) are adapted from Mander et al. [26]. In both of the used concrete material models, tension is not considered. Steel fibers behavior is determined using a simple bi-linear relationship for the tension part, and Dhakal and Maekawa [27] model for the compression part to include local bar buckling effects (Fig. 3b).

Material models for confined, unconfined concrete and reinforcement steel are regularized as suggested by Pugh et al. [28] to minimize dependency on mesh size. The ultimate strain values were determined using energy-based formulas [28] to prevent localization of deformation at critical fiber sections. These ultimate values are very important in determining the failure rotation or displacement of the RC columns and defining a correct limit state values. The column is considered to be failed when the analysis reaches concrete crushing value (ε_{cu}) or steel bars fractures at the ultimate strain (ε_{su}).

3.2 Shear and Slip Response

Predicting the shear and slip behavior of RC columns under lateral cyclic loading requires adding two springs in a zero-length element to the FBCEM as seen from Fig. 3a. In this study, Sezen shear model [29] is assigned to the horizontal spring representing the shear behavior of the column (Fig. 3). Additionally, a rotational spring is utilized to represent the slip response of the column. The Elastic material found in OpenSees library is allocated to the rotational slip spring, and Eq. 1 is used to calculate the slip stiffness as proposed by Elwood and Eberhard [30].

$$k_{\text{slip}} = \frac{8u}{d_l f_{yl}} E I_{\text{flex}} \tag{1}$$

In this equation, the average bond stress is taken as $u = 0.8\sqrt{f_{co}}$, and $E I_{\text{flex}}$ is obtained from the moment curvature analysis performed in OpenSees and expresses the stiffness up to the yielding moment.

Moreover, Hysteretic material from OpenSees was chosen because it reflects the shear model well. However, a simplification has to be applied to the four-point model of Sezen since the material consists of only three points. For that matter, the cracking point is not defined in the model. As defined in Fig. 4, the maximum strength point is selected as the minimum between the maximum shear strength V_n and maximum flexure strength V_p which determined as the ratio of the moment value at the time of formation of the plastic hinge to the shear span. Likewise, the maximum shear

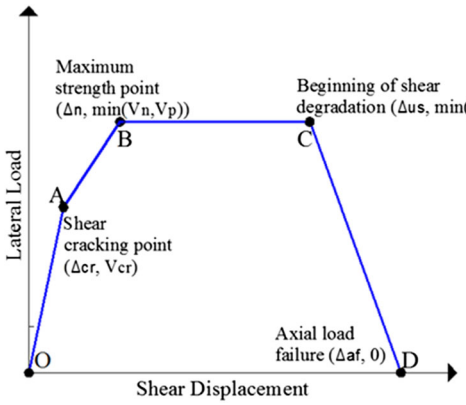

Fig. 4 Shear model proposed by Sezen [29]

strength V_n is calculated from Eq. 2.

$$V_n = k\frac{A_v f_{yh} d_{\text{eff}}}{s} + k\left(\frac{0.5\sqrt{f_{co}}}{L_s/d_{\text{eff}}}\sqrt{1+\frac{P}{0.5A_g\sqrt{f_{\text{co}}}}}\right)0.8A_g \tag{2}$$

In Eq. 2, A_v is the transverse reinforcement area, d_{eff} is the effective section depth, L_s is the shear span (moment/shear force ratio), A_g is the gross cross-sectional area, and k is a coefficient depending on the displacement ductility, where it is taken as 1 if the displacement ductility is less than 2, and 0.7 if the ductility is greater than 6, and for the intermediate values it varies linearly. Furthermore, the displacement value at the maximum strength Δ_n, and the deformation value at the moment when the shear strength starts to decrease Δ_{us} are calculated with the help of Eqs. 3 and 4, respectively. ρ_l given in this equation is the longitudinal reinforcement ratio.

$$\Delta_n = \left(\frac{f_{yl}\rho_l}{5000L_s/d_{eff}\sqrt{\frac{P}{A_g f_{\text{co}}}}} - 0.0004\right)L \tag{3}$$

$$\Delta_{us} = \left(4 - 12\frac{V_n}{bd_{\text{eff}} f_{co}}\right)\Delta_n \tag{4}$$

The value of the displacement at axial load failure Δ_{af}, as seen from Fig. 4, is determined by subtracting the maximum flexure and shear displacement from the total lateral displacement Δ_{ALF}. This value is calculated with the help of Eq. 5, where the angle of the shear fracture θ_a is accepted as 0.65, and d_c represents the depth of the core concrete.

$$\frac{\Delta_{\text{ALF}}}{L} = \frac{4}{100}\frac{1+\tan^2\theta_a}{\tan\theta_a + P\left(\frac{s}{A_v f_{yh} d_c \tan\theta_a}\right)} \tag{5}$$

4 Model Verification

For this work, displacement-based forceBeamColumn element and shear spring model were used to model the behavior of RC columns and a nonlinear finite element model was created. Experimental works selected from the literature (Table 1) were used to verify the nonlinear finite element model, and the models were analyzed under the effect of constant axial load and cyclic horizontal loading. The experimental results and the analysis results of the nonlinear finite element model are presented in Fig. 5 comparatively.

Furthermore, Table 2 summarizes the backbone values of the experimental and the numerical curves accumulated based on the definition from Fig. 6 [31]. In Table 2, $V_{\max}$,Δ_y, and Δ_u are the maximum lateral load, the displacements at yield, and at ultimate load (80% of $V_{\max}$), respectively. As seen from the table, although the initial stiffness is slightly over-estimated which is anticipated in numerical models in general, the results are consistence for all the specimens with a small error (7%). Moreover, the maximum error in the verification study is 11%, which acceptable in the literature [28] and shows clearly that the nonlinear finite element model can successfully simulate the behavior of RC columns under constant axial load and cyclic load.

5 Performance Limits in Codes

In this study, the deformation-based performance limits proposed by Eurocode 8, ASCE-SEI 41–17, and TBEC2018 have been examined in terms of rotational relationship under different axial load levels. As a result of the analysis performed for this purpose, the moment-chord rotation (Fig. 7) relationship of RC columns has been determined. In the numerical model, the RC column is fixed based, and fixed-roller top head, and this constraint arrangement was chosen to accommodate the experimental setups (Fig. 1). Chord rotation values were calculated by dividing the obtained displacement values by the column length (Fig. 7).

5.1 Eurocode 8 [3]

Equation 6 is used in Eurocode 8, to calculate the near collapse (NC) state limit. In this equation, γ_{el} is taken as 1.5 for a primary seismic element and 1 for a secondary seismic element. These values are chosen according to environmental conditions, but γ_{el} is chosen as 1 for this study. Axial load ratio is defined as $\vartheta = P/A_g f_{\text{co}}$. Mechanical reinforcement ratio of tension longitudinal bars is calculated as $w = A_{\text{sl}} f_{\text{yl}}/(A_g f_{\text{co}})$. The body reinforcements are included in the tension reinforcement area. Also, w' is the mechanical reinforcement ratio of the compressive longitudinal bars,

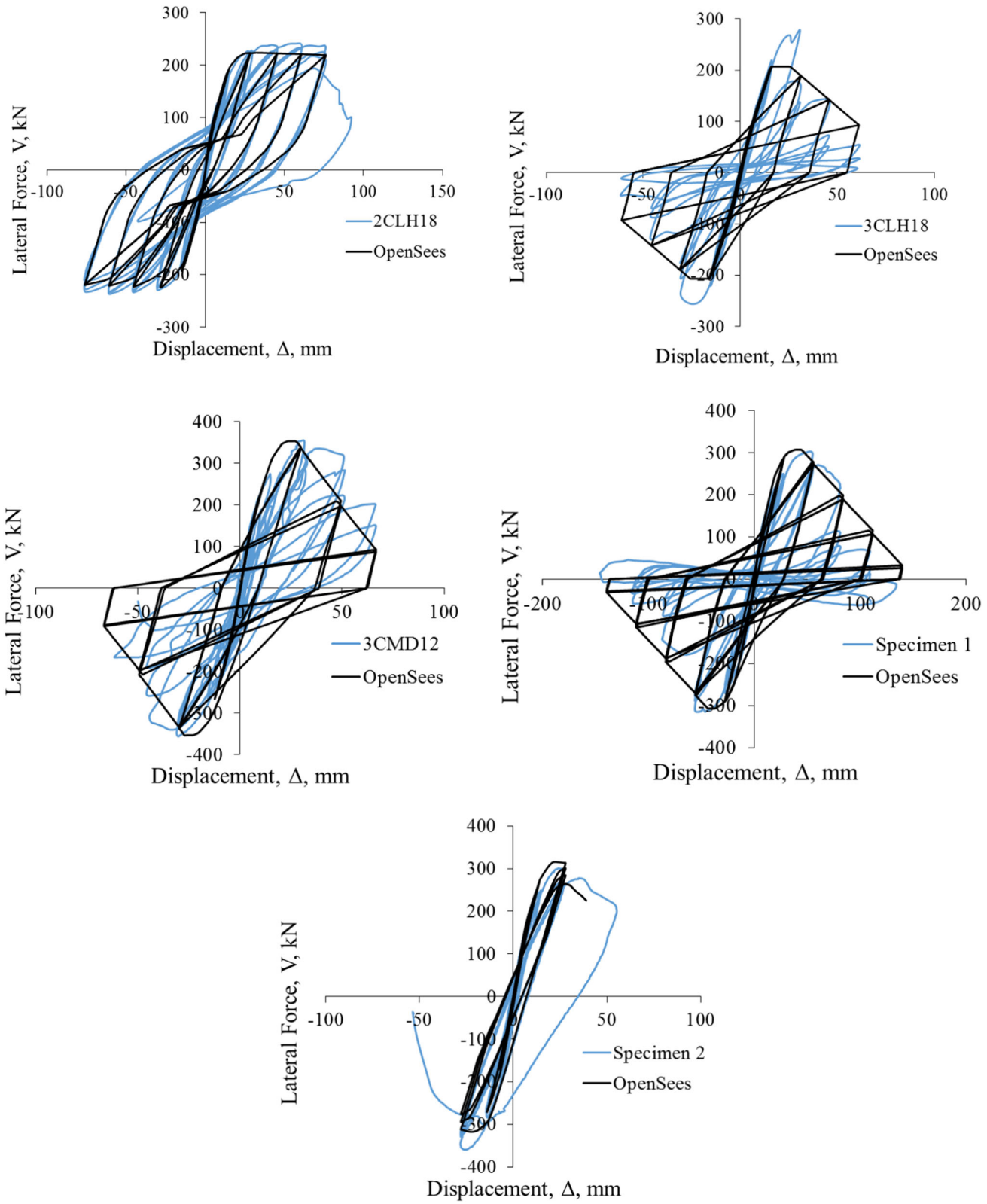

Fig. 5 Performance of the numerical model

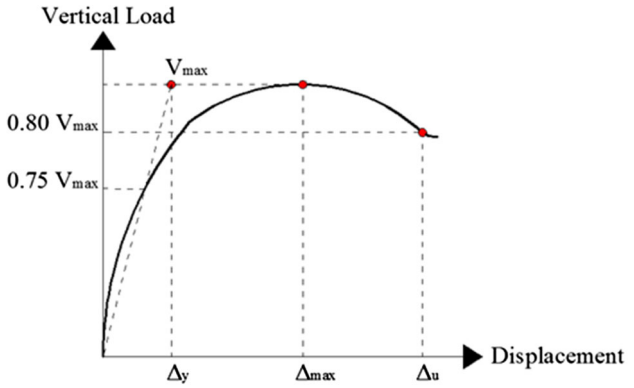

Fig. 6 Definition of main drifts points on the lateral load–displacement envelope

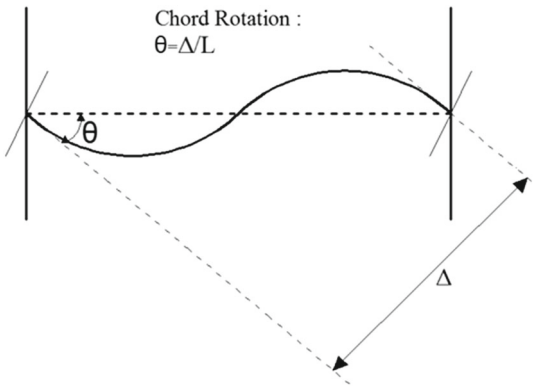

Fig. 7 Definition of chord rotation [10]

ρ_d diagonal reinforcement ratio, and α is the confinement effect factor which could be calculated using Eq. 7. The ratio of stirrups parallel to the loading direction is calculated as $\rho_{\mathrm{hx}} = A_{\mathrm{shx}}/(\mathrm{bs})$, where A_{shx} is the area of the horizontal reinforcement parallel to the loading direction. b_c and d_c given in Eq. 7 refer to the width and depth of the core concrete measured from the centers of the stirrups, respectively, b_i is defined as the distance between the centers of the horizontal reinforcement and the adjacent supported longitudinal reinforcement.

$$\theta_u = \frac{1}{\gamma_{el}} 0.016\left(0.3^{\upsilon}\right)\left[\frac{\max\left(0.01,\, w'\right)}{\max(0.01,\, w)} f_{co}\right]^{0.225} \times \left(\min\left(9,\, \frac{L_s}{d}\right)\right)^{0.35} 25^{\left(\alpha\rho_{hx}\frac{f_{yh}}{f_{co}}\right)}\left(1.25^{100\rho_d}\right) \tag{6}$$

$$\alpha = \left(1 - \frac{s}{2b_c}\right)\left(1 - \frac{s}{2d_c}\right)\left(1 - \frac{\sum b_i^2}{6b_c d_c}\right) \tag{7}$$

Moreover, the significant damage state limit (SD) is defined in Eurocode 8 as 0.75 of the collapse state limit. Two alternative equations (Eqs. 8 and 9) are proposed in Eurocode 8 and used in this study to determine the damage limitation bound (DL). In the equations, z is the stirrup arm in the cross section which can be taken as $0.8d$ or $\left(\mathrm{d_{eff}} - \mathrm{d}'\right)$. a_v is taken as 1 if the shear fracture exceeds flexural fracture; otherwise, it is taken as 0. Also, ε_{sy} is the unit deformation of the reinforcement at yield, d_{bl} diameter of the tension reinforcement, d_{eff} the tension reinforcement depth, and d' the compressive reinforcement depth.

$$\theta_y = \phi_y \frac{L_s + a_v z}{3} + 0.0014\left(1 + 1.5\frac{d}{L_s}\right) + \frac{\varepsilon_{\mathrm{sy}} d_{\mathrm{bl}} f_{\mathrm{yl}}}{\left(\mathrm{d_{eff}} - \mathrm{d}'\right) 6\sqrt{f_{\mathrm{co}}}} \tag{8}$$

$$\theta_y = \phi_y \frac{L_s + a_v z}{3} + 0.0014\left(1 + 1.5\frac{d}{L_s}\right) + \phi_y \frac{d_{\mathrm{bl}} f_{\mathrm{yl}}}{8\sqrt{f_{co}}} \tag{9}$$

5.2 ASCE-SEI 41–17 [10]

The plastic rotation limits of columns which are not controlled by in sufficient development length or overlapping are correlated with two coefficients in ASCE-SEI 41–17, a_{ASCE} and b_{ASCE} given in Eq. 10 and 11, respectively. a_{ASCE} cannot

Table 2 Validating the numerical model with the experimental results

Specimen	Δ_y^{exp} (mm)	Δ_y^{Num} (mm)	V_{max}^{exp} (kN)	V_{max}^{Num} (kN)	Δ_u^{exp} (mm)	Δ_u^{Num} (mm)	$\frac{\Delta_y^{Num}}{\Delta_y^{exp}}$	$\frac{V_{max}^{Num}}{V_{max}^{exp}}$	$\frac{\Delta_u^{Num}}{\Delta_u^{exp}}$
2CLH18	18.80	15.64	237.66	223.54	78.51	76.20	0.83	0.94	0.97
3CLH18	18.52	14.55	266.48	206.84	35.86	38.57	0.79	0.78	1.08
3CMD12	19.55	16.46	355.47	352.91	45.61	37.86	0.84	0.99	0.83
Specimen-1	28.22	23.39	308.61	306.81	66.97	65.69	0.83	0.99	0.98
Specimen-2	15.82	15.05	330.01	316.77	36.47	30.10	0.95	0.96	0.83
						Mean	0.85	0.93	0.94
						STD	0.06	0.09	0.11
						COV	0.07	0.10	0.11

take a value less than 0, and b_{ASCE} cannot take a value less than a_{ASCE}. ρ_h given in Eq. 10 is the ratio of horizontal reinforcement area to gross concrete area perpendicular to that reinforcement and must not be taken higher than 0.0175 and lower than 0.0075 in cases where it is not connected to the column core properly. Also, Eq. 10 is not valid for columns with $\rho_h < 0.0005$. Moreover, Eq. 11 is valid in situations where axial load ratio (ϑ) is smaller or equal to 0.5, which the case in this study.

$$a_{ASCE} = 0.042 - 0.043\vartheta + 0.63\rho_h - 0.023\left(\max\left(\frac{V_y}{V_o}, 0.2\right)\right) \tag{10}$$

$$b_{\mathrm{ASCE}} = \frac{0.5}{5 + \frac{P}{0.8A_g f_{\mathrm{co}}}\frac{1}{\rho_h}\frac{f_{co}}{f_{\mathrm{yh}}}} - 0.01 \tag{11}$$

The ratio of shear demand at flexural yielding to shear capacity (V_y/V_o) in Eq. 10, where V_y is obtained from the analysis and shear capacity (V_o) is calculated from Eq. 12. Herein, α_{col} is accepted as 1 for $s/d_{\mathrm{eff}} \leq 0.75$, whereas it is accepted as 0 for $s/d_{\mathrm{eff}} \geq 1$ and takes linear variation for values in between. λ is taken as 0.75 for slightly aggregated concrete and 1 for regular aggregated concrete. λ is accepted as 1 for the current study. Also, $M/(Vd_{\mathrm{eff}})$ ratio is defined as the rate of the largest produced moment to the shear force times effective depth and cannot be taken lower than 2 and higher than 4. The moment and shear values for RC columns are determined from the performed analysis.

$$V_o = k\left[\alpha_{\mathrm{col}}\frac{A_{\mathrm{sh}} f_{\mathrm{yh}} d_{\mathrm{eff}}}{s} + \lambda\left(\frac{0.5\sqrt{f_{\mathrm{co}}}}{M/(Vd_{\mathrm{eff}})}\sqrt{1 + \frac{P}{0.5\sqrt{f_{co}}A_g}}\right)0.8A_g\right] \tag{12}$$

Additionally, the plastic rotation limit for the immediate occupancy performance level (IO) is calculated as $0.15a_{ASCE}$ in ASCE-SEI 41–17, provided that it is less than or equal to 0.005. Also, the plastic rotation limit is calculated as $0.5b_{\mathrm{ASCE}}$ for the life safety performance level (LS) and $0.7b_{\mathrm{ASCE}}$ for the collapse prevention performance level (CP). To consider these values for LS and CP performance levels, the axial load ratio (ϑ) should be greater than 0.1. Likewise, ASCE-SEI 41–17 uses Eq. 13 to calculate the rotation at yield, where M_y represents the moment strength of the column cross section and L_p is taken as half of the column depth.

$$\theta_y = \frac{M_y}{EI_{\mathrm{flex}}}L_p \tag{13}$$

5.3 TBEC 2018 [7]

The yield rotation of the plastic hinge in TBEC 2018, θ_y, is calculated using Eq. 14. In this equation, ϕ_y is the effective yield curvature in plastic hinge and η is a constant which is accepted as 1 in columns. The effective yield curvature, ϕ_y, was obtained through moment curvature analysis performed on RC column cross sections using OpenSees program [16].

$$\theta_y = \frac{\phi_y L_S}{3} + 0.0015\eta\left(1 + 1.5\frac{d}{L_S}\right) + \frac{\phi_y d_l 1.2 f_{yl}}{8\sqrt{1.3 f_{co}}} \tag{14}$$

The plastic rotation value allowed for performance level of collapse prevention (CP), θ_p^{CP}, in TBEC 2018 is calculated using Eq. 15. The ultimate curvature value ϕ_u was also determined based on the moment curvature relation conducted in OpenSees using concrete and reinforcement steel models given in TBEC 2018. The length of plastic hinge L_p is accepted as half of the column depth.

$$\theta_p^{CP} = \frac{2}{3}\left[(\phi_u - \phi_y)L_p\left(1 - 1.5\frac{L_p}{L_s}\right) + 4.5\phi_u d_l\right] \tag{15}$$

Plastic rotation limit for controlled damage performance level (CD), θ_p^{CD}, is calculated as 75% of the plastic rotation limit given for the collapse prevention performance level in Eq. 15. Plastic rotation is not allowed for limited damage performance level (LD) if the effective section stiffness given in TBEC 2018 is used. In this study, plastic rotation was not allowed for the limited damage performance level.

6 Parametric Study

In the parametric study, three RC columns of different sizes were designed following the guidelines of TBEC 2018 [7] while considering the minimum requirements and design limits of Eurocode 8 and ASCE 41–17 building standards. Selected RC column sections, longitudinal reinforcement, and horizontal reinforcement properties are given in Fig. 8. The longitudinal reinforcement ratio of the RC columns was chosen as $\rho_l = 0.01$ and the volumetric ratio of stirrups as $\rho_h = A_{\mathrm{shx}}/(b_c s) = 0.007$ which were kept constant for all the samples. Additionally, column height was chosen as $L = 3000$mm, clear concrete cover was taken as 35 mm, and the concrete compressive strength as $f_{co} = 30MPa$. Also, the strength of the horizontal and longitudinal reinforcement used in the parametric study was chosen as $f_{\mathrm{sy}} = 420$MPa and $f_{\mathrm{su}} = 504MPa$ at yield and break, respectively, corresponding to the unit deformation at yield and break as $\varepsilon_{\mathrm{sy}} = 0.0021$ and $\varepsilon_{su} = 0.0800$, respectively.

In the parametric study, seven different axial load levels (0.10, 0.15, 0.20, 0.25, 0.30, 0.35 and 0.40) are applied to each one of the three RC column sections. Besides that, three cycles were applied for each lateral load level as shown in Fig. 9.

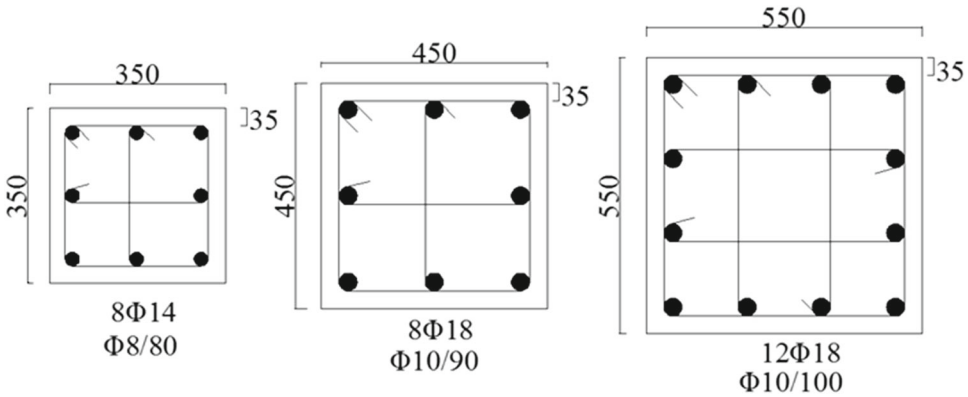

Fig. 8 Selected RC column sections

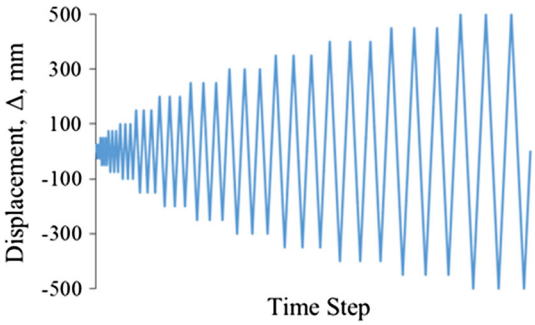

Fig. 9 Applied lateral loading

7 Results and Discussion

As a result of the performed analysis, performance level values of the RC columns under different axial loads are presented in Figs. 10, 11, and 12 for the limited damage, controlled damage, and collapse prevention performance limits, respectively. When the results are examined, all performance limit values defined in TBEC 2018 appear rather conservative in general compared to the values given in Eurocode 8 and ASCE 41–17.

As seen in Fig. 10, limited damage performance limits provide similar results with respect to all three codes and are well compatible with nonlinear FEM analysis results. Since all of three codes defined the controlled damage limit as a certain ratio of the collapse prevention limit, the discussion of the results was made in terms of collapse prevention. Collapse prevention performance values defined in TBEC2018 provide a cord rotation performance of approximately 1.75 times the Eurocode 8 limit values at columns with axial load ratio $\vartheta = 0.10$, and approximately 1.60 times at columns with axial load ratio $\vartheta = 0.40$. Collapse prevention performance limit values defined in TBEC2018 provide a cord rotation performance of approximately 1.80 times the ASCE 41–17 limit values at columns with axial load ratio $\vartheta = 0.10$ and approximately 1.20 times at columns with axial load ratio $\vartheta = 0.40$ (Fig. 12, Fig. 13, Table 3).

Moreover, as can be seen from Figs. 12 and 13, the collapse prevention performance limit values defined in TBEC 2018 are quite successful and compatible for all axial load ratios. Collapse prevention performance limit values defined in ASCE 41–17 are generally compatible with RC columns with axial load ratios between $\vartheta = 0.15$ and $\vartheta = 0.20$ which show flexure behavior, but are incompatible with RC columns with axial load ratio $\vartheta = 0.40$ (Fig. 13, Table 3). On the other hand, collapse prevention performance limit values defined in Eurocode 8 are highly compatible for RC columns showing flexural behavior with axial load ratios $\vartheta = 0.15$ and $\vartheta = 0.20$; however, they are not compatible with columns with $\vartheta = 0.30$ and above (Fig. 13, Table 3).

To test the performance of the values of the state limits proposed in the codes, Table 3 shows a comparison between the limit values set by the codes and the values obtained from the numerical analysis of the RC columns. In this table, values exceeding 90% of the realistic performance level are in bold font. However, the limit values calculated from the codes are expected to produce results that will stay on the safe side. The performance limits for the collapse prevention defined in TBEC2018 remain on the safe side for all axial load ratios, but remain very conservative for low axial load ratios and provide cord rotation performance around 20%–40%. It is clear that this situation may lead to an underutilization of the ductility property and flexural behavior of RC columns with a low axial load ratio. However, the performance limits for collapse prevention defined in TBEC2018 provide cord rotation performance of around 60–80% for high axial load ratios (Figs. 12 and 13, Table 3).

As seen in Fig. 12, Fig. 13 and Table 3, the collapse prevention performance limits defined in Eurocode 8 and ASCE 41–17 provide cord rotation performance around 50–70% for low axial load ratios. However, it is clear that the collapse prevention performance limits defined in Eurocode 8 and ASCE 41–17 are not on the safe side for high axial load ratios. Taking into consideration numerical analysis results obtained using the verified finite element model, it can be seen that

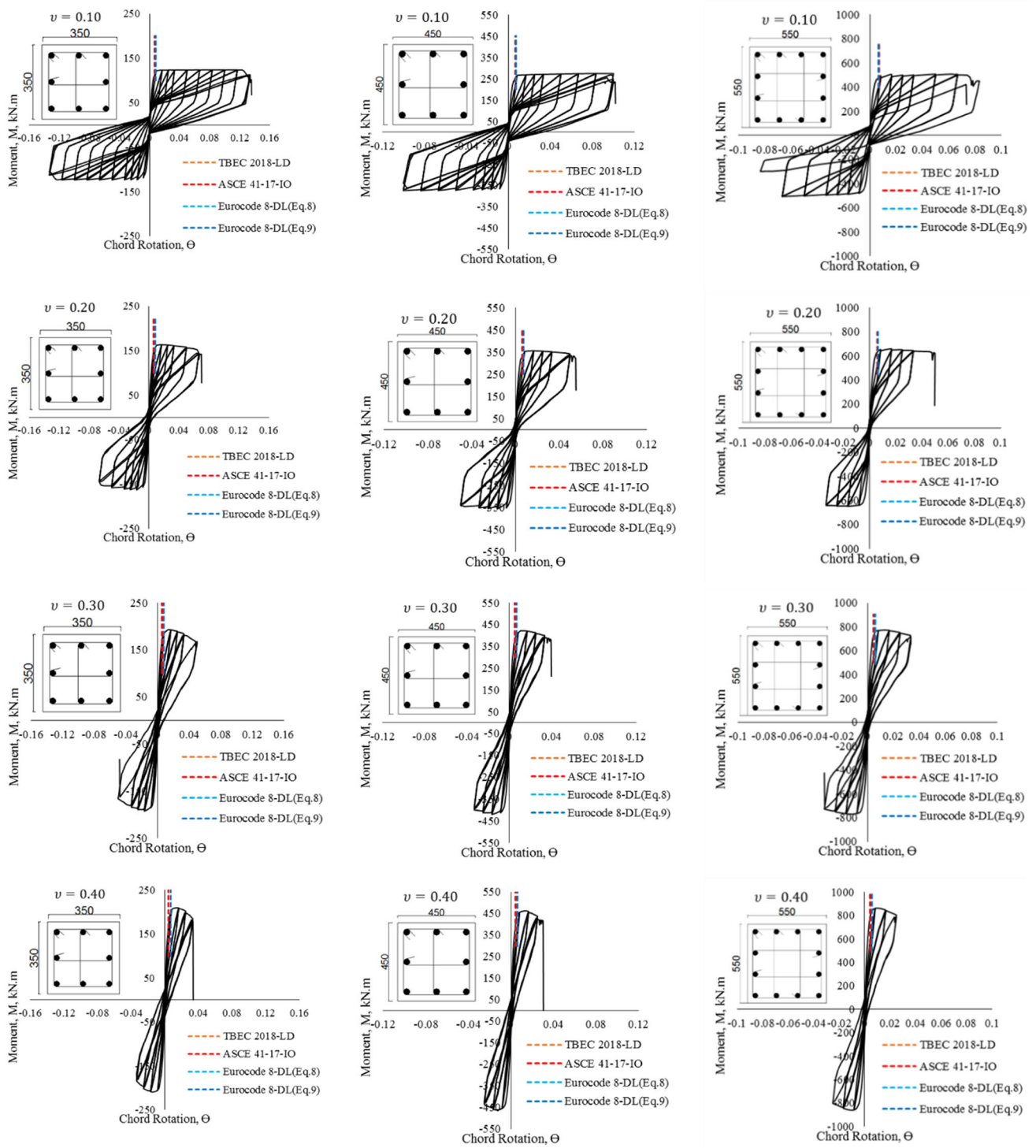

Fig. 10 Limited damage performance limits for RC columns

collapse prevention performance limits in codes are apparently exceeded for RC columns with axial load ratios higher than $\vartheta = 0.30$ in Eurocode 8 and $\vartheta = 0.35$ in ASCE 41–17. The bolded limit values in Table 3 clearly show that these values do not meet the requirement to collapse prevention and give results beyond the expected values.

As can be clearly seen from the results, the axial load level significantly affects the performance of RC columns subjected to earthquake loads. The performance limit values

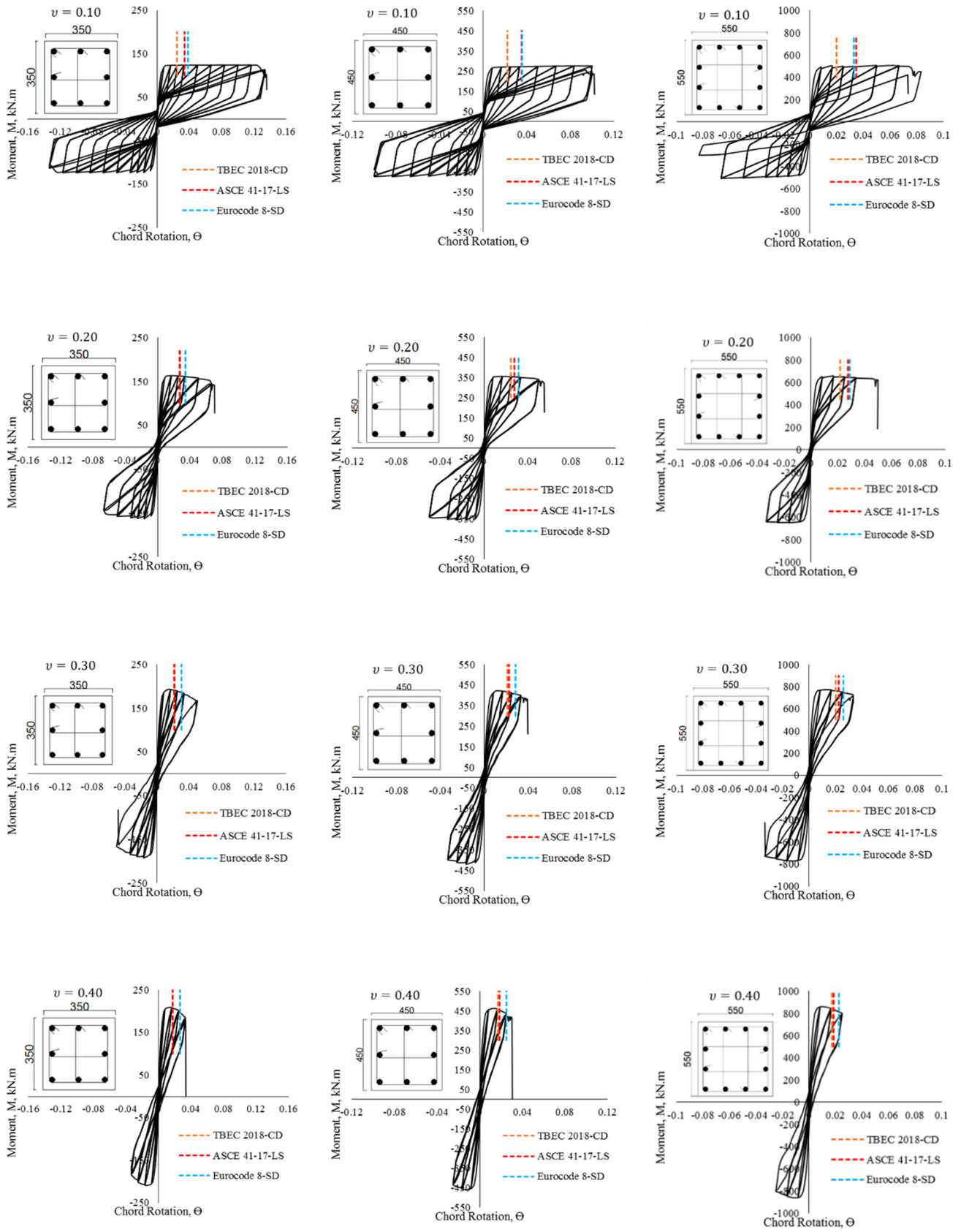

Fig. 11 Controlled damage performance limits for RC columns

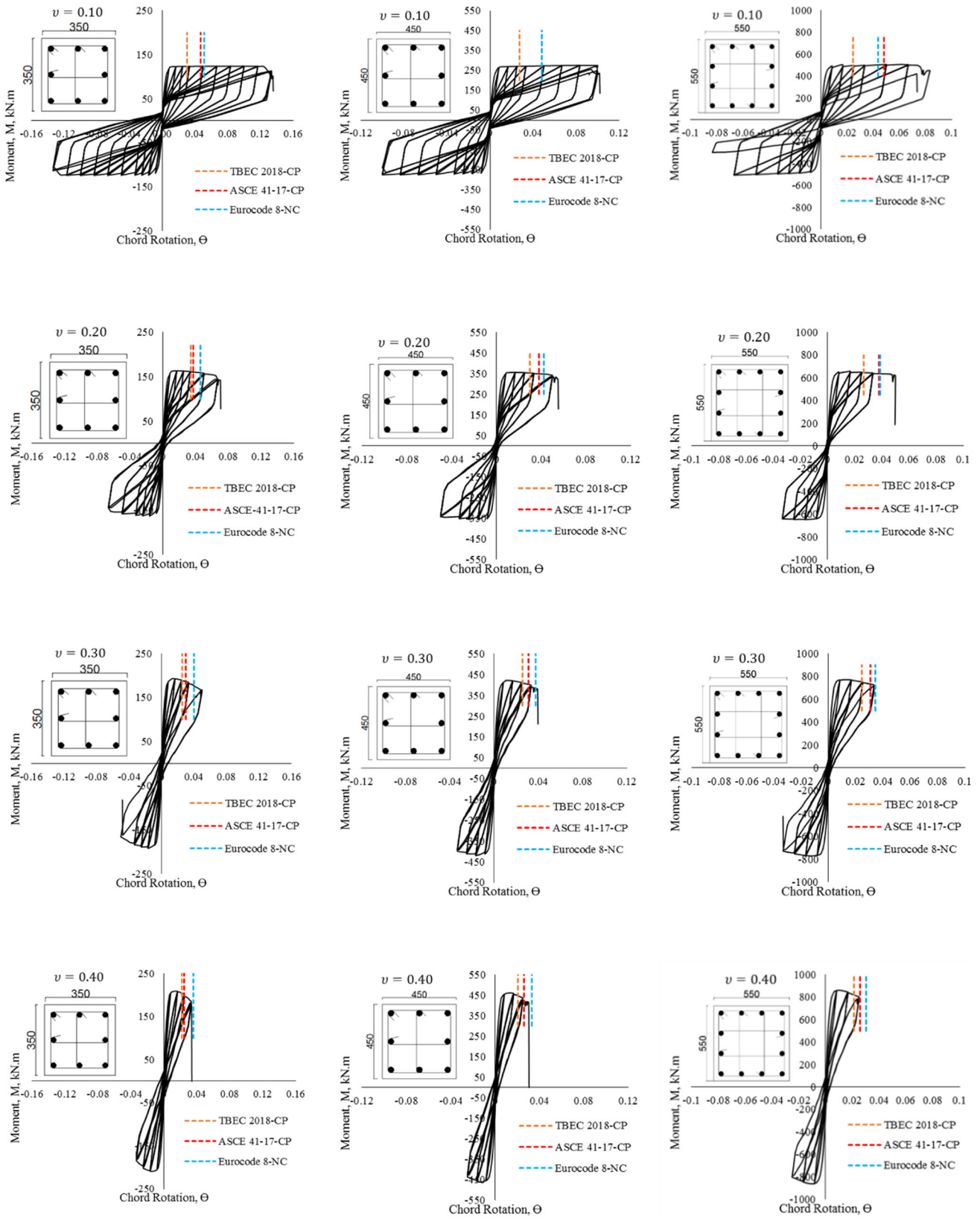

Fig. 12 Collapse prevention performance limits for RC columns

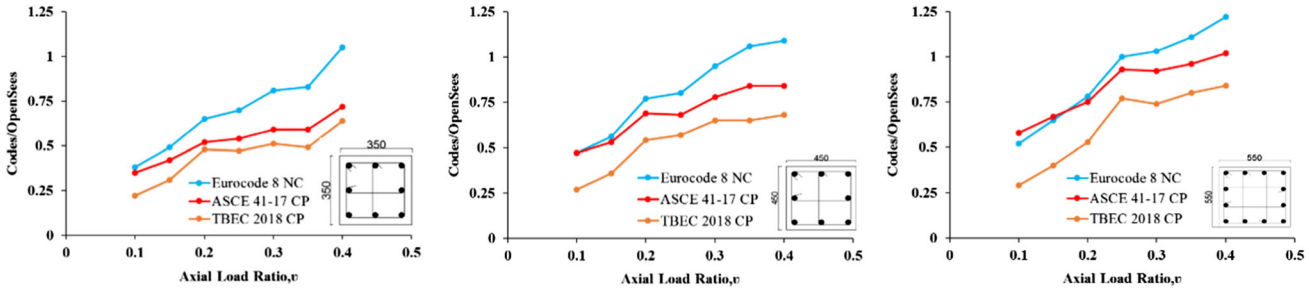

Fig. 13 Collapse prevention performance limit values according to axial load ratio

Table 3 Ratios of the collapse prevention performance limits for the RC columns

ϑ	TBEC2018 / OpenSees			EuroCode8 / OpenSees			ASCE41−17 / OpenSees		
	350 × 350 (mm)	450 × 450 (mm)	550 × 550 (mm)	350 × 350 (mm)	450 × 450 (mm)	550 × 550 (mm)	350 × 350 (mm)	450 × 450 (mm)	550 × 550 (mm)
0.10	0.22	0.27	0.29	0.38	0.47	0.52	0.35	0.47	0.58
0.15	0.31	0.36	0.40	0.49	0.56	0.65	0.42	0.53	0.67
0.20	0.48	0.54	0.53	0.65	0.77	0.78	0.52	0.69	0.75
0.25	0.47	0.57	0.77	0.70	0.80	**1.00**	0.54	0.68	**0.93**
0.30	0.51	0.65	0.74	0.81	**0.95**	**1.03**	0.59	0.78	**0.92**
0.35	0.49	0.65	0.80	0.83	**1.06**	**1.11**	0.59	0.84	**0.96**
0.40	0.64	0.68	0.84	**1.05**	**1.09**	**1.22**	0.72	0.84	**1.02**

for the collapse prevention defined in TBEC2018 are quite successful and compatible for high axial load ratios, while they remain quite conservative for low axial load ratios. The collapse prevention performance limits defined in Eurocode 8 and ASCE 41–17 are safe and compliant for low axial load levels, but not on the safe side for high axial load levels. Therefore, the limit values set by the codes should be re-evaluated and updated in terms of axial load ratios.

8 Conclusion

In this paper, the effectiveness of deformation-based performance limits proposed for RC columns in Eurocode 8, ASCE-SEI 41–17 and TBEC 2018 is examined quantitatively. In the first stage of the study, a nonlinear finite element model was developed and verified using results of experimental studies selected from the literature. It has been displayed that nonlinear finite element model successfully simulates the real behavior of RC columns under the impact of static axial load and repetitive lateral load.

In the second stage of the study, a parametric study was carried out to evaluate the performance of the state limits proposed in the codes. As a result, the following findings have been obtained:

- For all of the defined performance limits values, TBEC 2018 values are generally quite conservative compared to the values in Eurocode 8 and ASCE 41–17. As seen from the results, it is clear that this situation may lead to not fully utilize the potential ductile property and flexural capabilities of RC columns with low axial load ratios.
- The collapse prevention performance limits values defined in TBEC 2018 are considered to be very successful and compatible for all axial load ratios, since none of the code values exceeded 90% of the realistic results. However, the values defined in ASCE 41–17 and Eurocode 8 are generally not compatible for RC columns with axial load ratios higher than 25%.
- Limit values set by codes are expected to yield results that are on the safe side to a certain extent when compared to actual behavior. However, it has been determined that the collapse prevention performance limits defined in EuroCode 8 and ASCE 41–17 are not competent for RC columns with high axial load.
- It will be useful to re-evaluate and update the performance limit values defined by the codes in terms of axial load ratios, since the axial load level significantly affects the performance of RC columns subjected to earthquake loads.
- Although the maximum axial load level given in the codes is 0.40, as can be seen from the results, this value is critical to ensure the collapse prevention performance level.

Therefore, in order to stay on the safer side in the design of RC structures, the maximum axial load level should be re-evaluated and reduced.

- It should also be noted that the results of the study are only valid for the square RC columns with light reinforcement ratio ($\rho_l = 0.01$) and the volumetric ratio of stirrups as $\rho_h = 0.007$. For future research works, investigating columns with various shapes, sizes, and reinforcement ratios for longitudinal and transvers steel will be very useful for enhancing the performance levels specified in the codes for reinforced concrete columns.

References

1. Choi, M.H.; Lee, C.H.: Seismic behavior of existing reinforced concrete columns with non-seismic details under low axial loads. Materials **15**(3), 1239 (2022)
2. Acun, B.; Sucuoglu, H.: Evaluation of the performance limit states of reinforced concrete columns in view of experimental observations. IMO Tech. J. **22**(3), 5523–5541 (2011)
3. Comite Europeen de Normalisation (2005), "European Standard EN 1998–3 Eurocode 8: Design of Structures for Earthquake Resistance – Part 3: Assessment and Retrofitting of Buildings. Brussels
4. American Society of Civil Engineers: Seismic Rehabilitation of Existing Buildings: ASCE/SEI 41–06. American Society of Civil Engineers, Roston, VA (2007)
5. Specification for Structures to Be Built in Disaster Areas: TEC2018. Ministry of Public Works and Settlement, Ankara, Türkiye (2007)
6. Elci, H.; Goker, K.A.: Comparison of earthquake codes (TEC 2007 and TBEC 2018) in terms of seismic performance of RC columns. Int J Sci Technol Res **4**(6), 9–21 (2018)
7. Türkiye Building Earthquake Code:TBEC2018. Disaster and Emergency Management Presidency (AFAD), Ministry of Public Works and Settlement, Ankara, Türkiye (2018)
8. Opabola, E.; Elwood, K.J.: Comparative study on acceptance criteria for non-ductile reinforced concrete columns. Bull. N. Z. Soc. Earthq. Eng. **51**(4), 183–196 (2018)
9. American Society of Civil Engineers: Seismic Evaluation and Retrofit of Existing Buildins: ASCE Standard ASCE/SEI 41–13. American Society of Civil Engineers, Reston, VA (2014)
10. American Society of Civil Engineers: Seismic Evaluation and Retrofit of Existing Buildings, Standard ASCE/SEI 41–17. American Society of Civil Engineers, Reston, VA (2017)
11. Opabola, E.A.; Elwood, K.J.; Oliver, S.: Deformation capacity of reinforced concrete columns with smooth reinforcement. Bull. Earthq. Eng. **17**(5), 2509–2532 (2019)
12. Tore, E.; Demir, C.; Comert, M.; Ilki, A.: Seismic collapse performance of a full scale concrete building with lightly reinforced columns. J. Struct. Eng. **147**(12), 04021207 (2021)
13. Jamal, R.; Yuksel, S.B.: Comparison of performance analysis of a moment resisting framed structure according to TBDY 2018 and ASCE 41–17. El-Cezeri J. Sci. Eng. **8**(1), 432–444 (2021)
14. Foroughi, S.; Yuksel, S.B.: Investigation of deformation based damage limits of RC column. Int. J. Eng. Res. Dev. **11**(2), 584–601 (2019)
15. Foroughi, S.; Yuksel, S.B.: Investigation of deformation-based damage limits of RC columns for different seismic codes. J. Eng. Res. (2021)
16. McKenna, F.; Fenves, G.L.; Scott, M.H.: Open System for Earthquake Engineering Simulation (OpenSees). Pacific Earthquake Engineering Research Center University of California, Berkeley, CA (2000)
17. Sezen, H.: Seismic Behavior and Modeling of Reinforced Concrete Building Columns. University of California, Berkeley (2002)
18. Lynn, A.C.; Moehle, J.P.; Mahin, S.A.; Holmes, W.T.: Seismic evaluation of existing reinforced concrete building columns. Earthq. Spectra **12**(4), 715–739 (1996)
19. Martinelli, L.: Modeling shear-flexure interaction in reinforced concrete elements subjected to cyclic lateral loading. ACI Struct. J. **105**(6), 675–684 (2008)
20. Olabi, M.N.; Caglar, N.; Kisa, M.H.; Yuksel, S.B.: Numerical study on the response of composite shear walls with steel sheets under cyclic loading. J. Build. Eng. **34**, 102069 (2021)
21. Caglar, F.A.; Tatar, T.: Fiber based modeling strategies of RC columns. Acad. Platf. J. Nat. Hazards Disaster Manag **2**(2), 85–95 (2021)
22. Abadel, A.A.; Khan, M.I.; Masmoudi, R.: Experimental and numerical study of compressive behavior of axially loaded circular ultra-high-performance concrete-filled tube columns. Case Stud. Constr. Mater. **17**, e01376 (2022)
23. Spacone, E.; Filippou, F.C.; Taucer, F.F.: Fibre beam–column model for non-linear analysis of R/C frames: Part I. formulation. Earthq. Eng. Struct. Dyn. **25**(7), 711–725 (1996)
24. Zhu, M.; McKenna, F.; Scott, M.H.: OpenSeesPy: Python library for the OpenSees finite element framework. SoftwareX **7**, 6–11 (2018)
25. Kent, D.C.; Park, R.: Flexural members with confined concrete. J. Struct. Div. **97**(7), 1961–1990 (1971)
26. Mander, J.B.; Priestley, M.J.N.; Park, R.: Theoretical stress-strain model for confine concrete. J. Struct. Eng. **114**(8), 1804–1826 (1988)
27. Dhakal, R.P.; Maekawa, K.: Modeling for postyield buckling of reinforcement. J. Struct. Eng. **128**(9), 1139–1147 (2002)
28. Pugh, J.S.; Lowes, L.N.; Lehman, D.E.: Nonlinear line-element modeling of flexural reinforced concrete walls. Eng. Struct. **104**, 174–192 (2015)
29. Sezen, H.: Shear deformation model for reinforced concrete columns. Struct. Eng. Mech. **28**(1), 39–52 (2008)
30. Elwood, K.J.; Eberhard, M.O.: Effective stiffness of reinforced concrete columns. ACI Struct. J. **106**(4), 476 (2009)
31. ACI 374.2R. (2013). Guide for Testing Reinforced Concrete Structural Elements Under Slowly Applied Simulated Seismic Loads. In: 374.2 R-13. American Concrete Institute